Spectral properties of strongly perturbed Coulomb systems: Fluctuation properties

A. Hönig
Fakultät für Physik, Albert-Ludwigs-Universität, Hermann-Herder-Strasse 3, D-7800 Freiburg, West Germany

D. Wintgen
Max-Planck-Institut für Kernphysik, Postfach 103980, D-6900 Heidelberg, West Germany
(Received 21 December 1988)

We study the fluctuation properties of large-scale quantum spectra of the hydrogen atom in a uniform magnetic field. The present data are of a statistical significance not reached by any other study of these topics. This allows us to tackle a number of problems, whose treatment has been prevented hitherto by the lack of sufficiently long spectral sequences. We mainly focus on the dependency of fluctuation properties on the parameter describing the classical transition from regularity to irregularity. Our results strongly indicate that there are no universal distributions for the nearest-neighbor spacings in the transition regime. Generally, fluctuation measures can show extraordinary behavior, which can be understood only by a detailed knowledge of the underlying classical dynamics rather than by a knowledge of the global classical phase-space structure.

I. INTRODUCTION

This is the first of two planned papers which will deal with spectral properties of strongly perturbed Coulomb systems. We will give a comprehensive description of both fluctuation properties in this paper and long-ranged correlation properties in the planned companion paper.[1] Most of the spectra analyzed refer to the hydrogen atom in a uniform magnetic field. Recent progress in experimental and computational techniques has elevated this system to one of the best evaluated Coulomb and perhaps even general "complex" quantum system to date.[2–18]

An analysis of level spectra by statistical methods is the natural approach when the spectra are too complex to be analyzed level by level. Spectra can be separated quite generally into a smoothly varying average part and a fluctuating part describing the deviations from the average. The statistical analysis then concentrates on the fluctuating part. The characterization of these level fluctuations has received much interest in the past years. It has been conjectured[19] that complex systems exhibit universal fluctuation properties. This conjecture is supported now by the results of a large number of studies dealing with both experimental[20–26] and theoretical spectra.[27]

Much interest has centered on the question of how complex a system must be to obey the universal fluctuation laws. The results to date indicate that it is sufficient to have a (Hamiltonian) system with at least two degrees of freedom. Universal fluctuation properties then occur when the corresponding classical system is either integrable (random number fluctuations) or chaotic (or ergodic) (random matrix fluctuations). Thus the appearance of universal fluctuation patterns in quantum spectra is linked to the global structure of the underlying classical dynamics.

It often occurs, however, that the classical dynamics of a Hamiltonian system are neither chaotic nor integrable, but regular and irregular motion coexist. In fact, this seems to be the general case. Spectral fluctuations of Hamiltonian systems having a mixed phase space structure have been studied in the literature.[28–33] Nevertheless, the knowledge of their spectral properties is far from complete. All that is known is that their fluctuations are intermediate between the limiting universal patterns, Poisson and random matrix.

Perturbed Coulomb systems are ideally suited for the study of spectral properties. One major advantage is that they are often "real" and can be studied in the laboratory. Furthermore, the relevant interactions are usually known to a high precision and this may enable the performance of classical and quantum calculations without any approximation of the system under study. Spectra of Coulomb systems often consist of infinitely many bound levels *and* a structured continuum which results in a wealth of possible effects occurring. The classical dynamics of a perturbed Coulomb system may also show an unexpected behavior because the Kol'mogorov-Arnol'd-Moser theorem[34] is not applicable for pure Coulomb systems. Hence, all kinds of behavior may occur by addition of a perturbation; the system may remain regular (e.g., Stark effect[35]), it may display a smooth transition to chaos (e.g., the hydrogen atom in a uniform magnetic field[2,3]), or it may become ergodic at once (e.g., the anisotropic Kepler problem[36,37]).

In this paper we will concentrate on the spectral fluctuation properties of a hydrogen atom in a uniform magnetic field in the transition regime between regularity and irregularity. The results complement preliminary data on the nearest-neighbor spacing distributions[32] and gives new results for various fluctuation measures not considered so far. The data is of a statistical significance not reached in any previous study of these topics. This allows us to tackle a number of problems whose study has been inhibited so far by the lack of sufficiently long spectral sequences, e.g., $\hbar$ dependencies of fluctuations and

the behavior of the nearest-neighbor spacing distribution for small spacings.

The paper is organized as follows. We will introduce fluctuation measures in Sec. II and fluctuation models in Sec. III. This is done quite briefly and we refer to review articles giving more detailed information.[27,38–40] Section IV gives a brief description of the physical model under consideration, viz., the hydrogen atom in a uniform magnetic field. For more details we again refer to recent review articles.[2,3] Section V gives the results which are summarized and concluded in Sec. VI.

II. FLUCTUATION MEASURES

In this part we will briefly introduce the measures frequently used to characterize level fluctuations. Let us consider a discrete spectrum of levels $\{E_i\}$. Let $N(E)$ be the spectral staircase function which counts the number of levels below E. $N(E)$ consists of an average part and a fluctuating part,[41]

$$N(E)=N_{\rm av}(E)+N_{\rm fl}(E) . \tag{1}$$

Asymptotically, the average part is given by the semiclassical rule, that each quantum state of a d-dimensional system occupies a volume $(2\pi\hbar)^d$ of the total phase space Γ,

$$N_{\rm av}(E)\approx\Gamma(E)/(2\pi\hbar)^d . \tag{2}$$

Equation (2) can be used[19] to separate the fluctuating part of the level sequence $\{E_i\}$ by the transformation

$$\{\varepsilon_i\}=\{N_{\rm av}(E_i)\} . \tag{3}$$

The level sequence $\{\varepsilon_i\}$ now has unit mean spacing. In the following all fluctuation measures will apply to this sequence instead of $\{E_i\}$.

We are now able to define spectral fluctuation measures.[38]

(i) The distribution $P(s)$ of spacings s between adjacent levels [nearest-neighbor spacing (NNS) distribution]. The NNS distribution is simply the probability P for finding a separation s of neighboring levels in the spectrum.

(ii) The number statistic $n(L)$ of the distribution and the moments associated with it. Given an interval $[\alpha,\alpha+L]$ of length L, $n(\alpha,L)$ counts the number of levels within this spectral range. Averaging over the spectrum (i.e., over α) yields the moments of the distribution. Here we consider the leading moments: variance $\Sigma_2(L)$, skewness $\gamma_1(L)$, and excess $\gamma_2(L)$.[42] The first moment (mean value) is simply L, because the mean spacing is unity. Qualitatively we expect that the variance Σ_2 is small if the spectrum is stiff and large otherwise.

(iii) Spectral rigidity Δ_3 of the spectrum. Given a substretch $[\alpha,\alpha+L]$ of the spectrum, it measures the least-square deviation of the spectral staircase function from the best straight line fitting it,

$$\Delta_3(L;\alpha)=\frac{1}{L}\min_{A,B}\int_{\alpha}^{\alpha+L}[N(\varepsilon)-A\varepsilon-B]^2d\varepsilon . \tag{4a}$$

Note that through the transformation (3) we are dealing with spectra whose average part is the identity, $N_{\rm av}(\varepsilon)=\varepsilon$, but for a finite interval $[\alpha,\alpha+L]$ the best straight line fit to $N_{\rm av}+N_{\rm fl}$ may differ slightly. Averaging over the spectrum gives the rigidity $\Delta_3(L)$. Δ_3 is connected to the variance Σ_2 by an integral transformation,[43,44]

$$\Delta_3(L)=\frac{2}{L^4}\int_0^L dx(L^3-2L^2x+x^3)\Sigma_2(x) . \tag{4b}$$

A convenient way to calculate Δ_3 is given in Bohigas and Giannoni.[38]

III. FLUCTUATION MODELS

A. Universal fluctuation models

The functional forms of the measures introduced in Sec. II are known analytically for some specific model spectra. Two kinds of spectra are particularly important: (a) (uncorrelated) random level spectra (Poisson spectrum) and (b) random matrix spectra. In the latter case one has to distinguish between real symmetric [Gaussian orthogonal ensemble (GOE)] and complex Hermitian random matrices [Gaussian unitary ensemble (GUE)].[44] Spectra belonging to the preceding classes share universal fluctuation properties. Their spacing distributions are given by

$$P(s)=\begin{cases} e^{-s} \ \text{(Poisson)} & \text{(5a)} \\ \dfrac{\pi}{2}se^{-(\pi/4)s^2} \ \text{(GOE)} & \text{(5b)} \\ \dfrac{32}{\pi^2}s^2e^{-(4/\pi)s^2} \ \text{(GUE)} . & \text{(5c)} \end{cases}$$

[Eqs. (5b) and (5c) represent approximations which deviate only very slightly from the exact distributions.] The Poisson distribution can be obtained by a maximal entropy consideration under the constraints of normalization $[\int_0^\infty P(s)ds=1]$ and unit mean spacing normalization $[\int_0^\infty sP(s)ds=1]$. Both the Poisson (5a) and the Wigner (5b) distribution can be derived from a simple probability argument, which results in an integral equation for the distribution $P(s)$,[44]

$$P(s)=r(s)\int_s^\infty P(x)dx . \tag{6}$$

The Poisson law follows if we take the level repulsion function $r(s)$ to be unity (no level repulsion), whereas Wigner's law follows from the assumption of linear repulsion $r\sim s$. In fact, the essential difference of the distributions (5) is their behavior at small spacings s. While degeneracy of levels ($s=0$) is the most probable spacing for the Poisson case (5a), random matrix spectra show linear (quadratic) repulsion for the GOE (GUE) case, i.e., the tendency to avoid level clustering.

The spectral rigidity Δ_3 is given asymptotically ($L\gg1$) by

$$\Delta_3 \approx \begin{cases} L/15 \quad \text{(Poisson)} \\ \frac{1}{\pi^2}\ln L - 0.007 \quad \text{(GOE)} \\ \frac{1}{2\pi^2}\ln L + 0.059 \quad \text{(GUE)} . \end{cases} \tag{7}$$

The expression for the Poisson case is valid for all L. Analytic random matrix expressions valid for all L can be found in Brody *et al.*[44] and Bohigas and Giannoni.[38]

Analytic formulas for the higher moments, skewness and excess, are too complicated to be listed here. They can be found in Bohigas *et al.*[23] A graphical presentation of them will be given when discussing results in Sec. V.

Originally, analyses in the spirit of random matrix theories applied to complex systems with many degrees of freedom, where a statistical treatment is not only natural but the only feasible one. However, further physical significance of the theory stems from the following conjecture which was formulated first by Bohigas *et al.*:[19] Spectral fluctuations of classically chaotic systems coincide with GOE (GUE) fluctuations, if the system is (not) time-reversal invariant, whereas spectral fluctuations of classically integrable systems coincide with Poisson fluctuations.

Apart from the very large numerical evidence for this conjecture, some progress has been made in putting it on a firm mathematical footing. We mention here a semiclassical derivation of the spectral rigidity by Berry,[45] which coincides with random matrix predictions (see Sec. III C). A further generalization of the concept of time reversibility in terms of antiunitary symmetries was given by Berry and Robnik.[46] The fact, that "chaotic" quantum spectra share the same universal fluctuation properties as random matrices does not mean that they are indistinguishable from random matrix spectra, as was shown explicitly by Wintgen.[10] The reason is that most of the fluctuation measures defined in Sec. II are short-range sensitive and do not include correlations of levels extending over spectral ranges larger than L. The coincidence of the statistics should be understood as a local rather than a global property of the spectra.

B. Models for generic spectra

Generally the classical dynamics of a Hamiltonian system is neither regular nor chaotic, but both types of motion coexist.[47] What is known about these systems is that they obey spectral fluctuations intermediate between Poisson and random matrices. It has been argued that no universal distributions exist for these systems.[48] Numerical studies have shown, however, that spectral properties of such systems look very similar, supporting the idea that they can be described at least approximately by common distributions. Various families of distributions have been proposed to fit the NNS distributions for these systems. They depend on one parameter (or more), which can be tuned to interpolate between the limiting cases of regular and irregular spectra. In the following we summarize some of them.

The Brody distribution is given by[49]

$$P(s) = \alpha(q+1)s^q e^{-\alpha s^{q+1}} , \tag{8}$$

with

$$\alpha = \left[\Gamma\left[\frac{q+2}{q+1} \right] \right]^{q+1} .$$

The distribution interpolates between the Poisson distribution ($q=0$) and the (GOE) Wigner distribution ($q=1$). It can be derived by assuming the power-law level repulsion $r \sim s^q$ in Eq. (6).

The Berry-Robnik distribution[50]

$$P(s) = e^{(q-1)s}\left[(1-q)^2 \operatorname{erfc}\left[\frac{\sqrt{\pi}}{2} qs \right] + \left[2q(1-q) + \frac{\pi}{2} q^3 s \right] e^{-(\pi/4)q^2 s^2} \right] \tag{9}$$

also interpolates between the Poisson ($q=0$) and the Wigner ($q=1$) distribution. The distribution is obtained by superimposing an irregular spectrum obeying Wigner statistics with a regular spectrum obeying Poisson statistics. Their relative weights q and $1-q$ are given by the fraction q of classical phase space, which is irregular. A prominent feature of this distribution is its nonvanishing value for $s=0$ (as long as $q \neq 1$), reflecting the absence of level repulsion between the two *different sources* of superimposed levels.

More recently another formula has been proposed by Hasegawa *et al.*,[51] who applied a stochastic differential equations approach to the level motion theory, which was introduced in this context by Pechukas[52] and further developed by Yukawa.[53] Their distribution depends on two parameters, λ and α, and reads

$$P(s) = N\rho s(\rho^2 s^2 e^{2\rho s} + \lambda^2 e^{\alpha^2 \rho^2 s^2})^{-1/2} , \tag{10}$$

with ρ and N given by

$$\rho = F_2/F_1 ,$$

$$N = \rho/F_1 ,$$

$$F_n = \int_0^\infty x^n (x^2 e^{2x} + \lambda^2 e^{\alpha^2 x^2})^{-1/2} dx .$$

The underlying idea is that there are two different types of noise in the system, one responsible for level clustering, and the other responsible for level repulsion. The parameter λ measures the relative strength of the two types of noise, whereas the ratio of the average level densities associated with the noises is governed by α. For $\lambda=0$ Eq. (10) reduces to the Poisson distribution, whereas the Wigner distribution is obtained in the limit $\lambda \to \infty$.

We have investigated two further distributions, but with limited success. The first one was proposed by Robnik.[48] He derived $P(s)$ from a maximal entropy consideration under the additional constraint that the second moment $\langle s^2 \rangle = \int_0^\infty s^2 P(s) ds$ of the distribution is prescribed. However, we found that the resulting distribution

$$P(s) = s e^{\lambda + \mu s + \nu s^2} \tag{11}$$

is unable to reproduce the regular Poisson case (λ, μ, and ν are determined by fixing the leading moments, $\langle 1 \rangle$, $\langle s \rangle$, and $\langle s^2 \rangle$, to their correct values).

The second distribution, not considered so far in the literature, is obtained by setting the repulsion function $r(s)$ in Eq. (6) to

$$r(s) \sim \frac{s}{(s^2+q^2)^{1/2}} .$$

Again this repulsion function interpolates between Poisson ($q=0$) and Wigner ($q \to \infty$) and the corresponding NNS distribution reads

$$P(s)=N\frac{s}{(s^2+q^2)^{1/2}}\exp[-\alpha(s^2+q^2)^{1/2}] , \tag{12}$$

where N and α are determined by normalization. The distribution depends linearly on s for small spacings $s \ll q$. Although it possesses the correct limiting forms, fits to the computed spectra studied below were generally poor compared to fits with the Brody formula. Therefore we do not refer further to this distribution. The same state of affairs holds for the Berry-Robnik distribution (9), which fails to describe the computed spectra for small spacings, although the physical idea behind the formula is very promising (see also Sec. V).

In addition to the distributions proposed above we calculated the "real" NNS distribution $P(s)$ of a given spectrum. By real we mean a smooth approximation to the observed distribution

$$P(s)=\frac{1}{M}\sum_{i=1}^{M}\delta(s-s_i) . \tag{13}$$

We obtain a smoothed version of Eq. (13) by expanding $P(s)$ in the complete set of basis functions $\Phi_n(s) = L_n(2s)e^{-s}$, where L_n are the usual Laguerre polynomials,[54]

$$P(s)=\sum_{n\,(n\le n_0)} c_n\Phi_n(s) . \tag{14}$$

The cutoff value n_0 can be determined by the requirement that the distribution (14) should image the cumulative distribution within some given accuracy. The distribution $P(s)$ rapidly converges with increasing n_0. (Note that the Poisson distribution is recovered by the $n=0$ term only.) By inappropriately increasing n_0 the distribution tries to resolve fine-structure components of the real distribution which often are statistically insignificant and which are desired to be eliminated. In practice the expansion (14) works very well and a typical cutoff value is $n_0 \approx 12$. The distributions (14) become nearly indistinguishable for cutoff values near n_0. Although Eq. (14) is of no great practical use in parametrizing $P(s)$, in particular in giving the expansion coefficients c_n any physical meaning, the procedure enables one to get rid of the usual histogram representation of the NNS distribution. Unfortunately it is often the case that the overall agreement between the real distribution and some fit distribution can be manipulated by a proper choice of the histogram step size. Alternatively, the differences between the more or less smooth cumulative spacing distributions are not as dramatic as the differences in the distributions themselves. Hence a comparison between the proposed, Eqs. (8)–(12), and the "exact" distributions, Eq. (14), is the most objective choice.

A model for the Δ_3 (and analogously for the Σ_2) statistic in the intermediate regime is given by the independent superposition of a regular Poisson spectrum with weight q and an irregular GOE spectrum with weight $q'=1-q$. This leads to[44]

$$\Delta_3(L;q)=\Delta_3^{\text{Poisson}}(qL)+\Delta_3^{\text{GOE}}(q'L) , \tag{15}$$

$$\Sigma_2(L;q)=\Sigma_2^{\text{Poisson}}(qL)+\Sigma_2^{\text{GOE}}(q'L) . \tag{16}$$

To derive analogous expressions by simply scaling the arguments is no longer possible for γ_1 and γ_2 and the corresponding formulas are more complicated.[55]

C. Nonuniversal behavior: Semiclassical models

All the distributions presented in the previous sections are derived from a statistical point of view involving physically more or less justified assumptions. What would be more satisfactory is a derivation from first principles, i.e., from a quantum-mechanical or a semiclassical starting point. Progress in this direction has been achieved mainly by Berry, who derived semiclassical formulas for the spectral rigidity Δ_3 (Ref. 45) and the number variance Σ_2 (Ref. 56) (see also Verbaarschot[43]). In the following we will sketch the theory for Δ_3 and give the results.

The starting point of the theory is the semiclassical representation of the fluctuating part $N_{\text{fl}}(E)$ of the spectral staircase function (1) formulated by Gutzwiller,[57]

$$N_{\text{fl}}(E)=\frac{1}{\hbar^{(N-1)/2}}\sum_{r,j} A_{rj}(E)\exp[ijS_r(E)/\hbar] . \tag{17}$$

In the sum r labels all distinct primitive periodic orbits (and their multiple traversals j) having actions S_r. The amplitudes A_{rj} depend on various aspects of the particular orbit r, e.g., stability, period, etc. N is 1 for isolated orbits (this applies to all nonintegrable systems) and equal to the degrees of freedom for a nonisolated orbit of an integrable system. Equation (17) is used together with the definition of Δ_3, Eq. (4), to obtain the following general expression for the spectral rigidity:

$$\Delta_3(L)=\frac{1}{\pi}\int_0^\infty \frac{dt}{t}\frac{K(t/\hbar\bar{n}(E))}{t/\hbar\bar{n}(E)}G(Lt/2\hbar\bar{n}(E)) , \tag{18}$$

with $\bar{n}(E)$ being the mean level density dN_{av}/dE and G the *orbit selection function*,

$$G(y)=1-\frac{\sin^2 y}{y^2}-3\left[\frac{d}{dy}\frac{\sin y}{y}\right]^2 . \tag{19}$$

$K(t)$ is the spectral form factor, i.e., the Fourier transform of the correlation function of the spectral density. The difficulty is to determine the spectral form factor $K(t)$, which generally is characteristic of the physical system under consideration. However, the asymptotic behavior of K is known and depends only on global as-

pects of the classical dynamics,[58] e.g., global phase-space structure, time reversibility, etc. The expression (18) can now be evaluated by splitting the integral and exploiting the asymptotic properties of K and G. However, care has to be taken when considering the asymptotic behavior of the orbit selection function, since its argument explicitly depends on the mean density of states $\bar{n}$. Thus one can distinguish two regions, $L \ll L_{\max}$ and $L \gg L_{\max}$. $L_{\max}$ is given by

$$L_{\max}=2\pi\hbar\bar{n}(E)/T_{\min} , \tag{20}$$

where $T_{\min}$ is the period of the shortest classical closed orbit. For $L \ll L_{\max}$ the evaluation of the integral (18) yields the same L dependence as given in Eq. (7), thus providing a semiclassical justification for a random matrix ansatz. The constant terms in Eq. (7) are obtained when setting $K(t)$ to the appropriate random matrix form factors, whose asymptotic behavior coincide with the semiclassical ones. For $L \gg L_{\max}$ the integral (18) saturates to a nonuniversal value Δ_∞, which is given approximately by[45]

$$\Delta_\infty=\frac{2}{\hbar^{N-1}}\sum_{r,j} A_{rj}^2 . \tag{21}$$

In between the two limits, i.e., $L \approx L_{\max}$, a weak oscillatory structure may be imposed on the saturating distribution.

For the number variance Σ_2 a semiclassical analysis has been done in the same spirit. Here, we only quote the result,[56]

$$\Sigma_2(L)=\frac{8}{\hbar^{N-1}}\left[\sum_{r,j} A_{rj}^2 \sin^2[jLT_r/2\hbar\bar{n}(E)]\right] . \tag{22}$$

Again, the asymptotic part of the sum (long orbits) can be approximated by a universal random matrix ansatz. In contrast to the asymptotic *saturation* of the spectral rigidity Δ_3, the nonuniversal asymptotic behavior of the number variance Σ_2 consists of a (quasirandom) oscillation pattern.[43,56] Semiclassical formulas for higher moments can be found in Verbaarschot.[43]

IV. DERIVATION OF THE SPECTRA

Before we discuss our results in Sec. V, a short description of the underlying physical system is necessary. The quantum spectra for our analysis are derived by solving the Schrödinger equation for the hydrogen atom in a uniform magnetic field, for which the Hamiltonian reads[2,3] (atomic units used)

$$H=\frac{p^2}{2}-\frac{1}{r}+\tfrac{1}{8}\gamma^2(x^2+y^2) . \tag{23}$$

The z axis is chosen as the direction of the magnetic field B, which is measured in units of $B_0=2.35\times10^5$ T, $B=\gamma B_0$. The trivial (since constant) paramagnetic term proportional to B is omitted in (23). The Hamiltonian (23) fails to separate in any coordinate system; only the azimuthal quantum number m and parity π are good quantum numbers and can be isolated. The Hamiltonian (23) scales as

$$H(\mathbf{p},\mathbf{r};\gamma)=\gamma^{2/3}H(\gamma^{-1/3}\mathbf{p},\gamma^{2/3}\mathbf{r};\gamma=1) , \tag{24}$$

with the scaled Hamiltonian being independent on the field strength γ. As a consequence the classical dynamics do not depend on energy and field strength separately, but depend only on the *scaled energy* ε,

$$\varepsilon=E\gamma^{-2/3} .$$

The properties of a hydrogen atom in a uniform magnetic field have been reviewed recently.[2,3] The classical system displays a smooth transition from regularity to chaos as the parameter ε is varied. This is demonstrated in Fig. 1, which shows Poincaré surfaces of section for $m=0$ and for six different values of the scaled energy ε: -0.8, -0.5, -0.4, -0.3, -0.2, and -0.1 (from left to right and from top to bottom). The surface of section is defined by recording and plotting the phase space coordinates $\nu=\sqrt{\bar{r}-\bar{z}}$ and its conjugate momentum p_ν whenever a classical trajectory passes through the $\rho=0$ axis. Regular classical motion is indicated by the existence of invariant manifolds (tori) on which the motion is confined

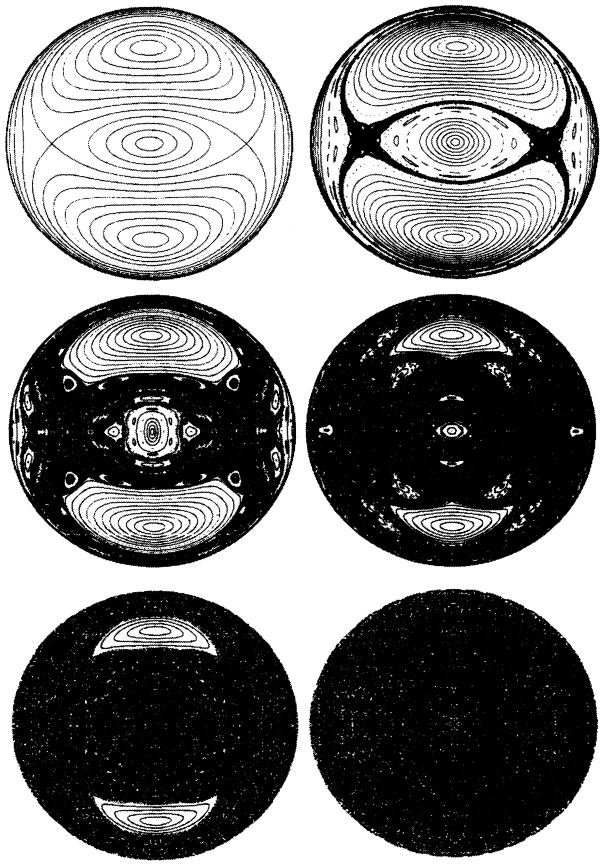

FIG. 1. Poincaré surfaces of section for the hydrogen atom in a uniform magnetic field for different values of the scaled energy ε: -0.8, -0.5, -0.4, -0.3, -0.2, and -0.1 (from left to right and top to bottom).

for all times, whereas a typical chaotic trajectory occupies a finite volume in phase space and a finite area in the surface of section. For $\varepsilon=-0.8$ the system behaves regularly and is hardly distinguishable from an integrable one. Classical chaotic motion first appears near the separatrix as we decrease (by absolute value) the scaled energy. By further decreasing ε the regular part of the phase space becomes smaller and smaller, until the last large regular island disappears at $\varepsilon=-0.127\,27$. The dependence of the classical dynamics on the scaled z component of angular momentum $\tilde{l}_z$ can be neglected for our purpose.[59]

The techniques to solve the Schrödinger equation for fixed values of the scaled energy ε are described in Ref. 59. First results on the statistical behavior of these spectra were reported in Refs. 7 and 32, where the nearest-neighbor spacing distributions (NNS) were studied for different values of ε. Spectral statistics (NNS and Δ_3, and very recently transition strengths fluctuations[60]) were also studied by Delande and Gay[8] and Wunner *et al.*,[9] who calculated quantum spectra at a fixed field strength γ instead of fixed scaled energy ε. As long as the classical dynamics are either completely regular or completely irregular these different approaches yield similar results, as demonstrated in Refs. 7–9. However, a study of the transition regime between regularity and irregularity can only be meaningful by fixing the classical dynamics, that is, the scaled energy ε.

In this paper we analyze 56 spectra at fixed scaled energies, ranging from $\varepsilon=-0.4$ up to $\varepsilon=-0.1$ in steps of 0.05. Spectra are obtained for eight different subspaces m^{π}, $m=0,1,2,3$, and both parities. A typical spectrum consists of 350 ($\varepsilon=-0.1$) up to 1600 levels ($\varepsilon=-0.4$). We required a convergence of the energy levels of at least 0.1% of the mean level spacing. After checking statistical independence of the calculated statistics in the various m^{π} subspaces, one can average them to increase the statistical significance. We have always done this, *if not* stated otherwise. The total number of levels for the various values of the scaled energy are listed in Table I.

Unfolding the spectra to unit mean level density as described in connection with Eqs. (2) and (3) was done numerically by fitting the spectral staircase function N by a second order polynominal in $\gamma^{-1/3}$. Then the coefficient of the leading term proportional to $\gamma^{-2/3}$ is given by the phase space volume in the scaled coordinates (24). We have checked this and generally found an agreement within the order of ppm between the calculated phase-space volume and the leading fit coefficient of the spectral staircase function.

TABLE I. Number N of converged eigenvalues for the different scaled energies ε.

ε	N
−0.10	2980
−0.15	4800
−0.20	6000
−0.25	8000
−0.30	9600
−0.35	11200
−0.40	12800

V. RESULTS AND DISCUSSION

A. Level statistics for irregular behavior

As is discussed in Sec. IV and shown in Fig. 1, the classical dynamics of a hydrogen atom in a uniform magnetic field turn out to be completely chaotic for $\varepsilon>-0.127\,27$. Hence spectra generated for $\varepsilon=-0.1$ are suitable to test the hypothesis of GOE fluctuations for classically chaotic systems. Although the full Hamiltonian *including* the paramagnetic term proportional to l_z is *not* invariant under a time-reversal transformation, we expect GOE rather than GUE fluctuations. The reason for this is that the concept of time reversibility must be replaced by a more general concept of antiunitary symmetries.[46] To be concrete, the effective Hamiltonian (23) is invariant under time reversal, and the full Hamiltonian is invariant under simultaneous time reversal *and* reflection through the (x,y) plane, thus yielding GOE instead of GUE fluctuations.

Figure 2 shows the results for the level statistics for $\varepsilon=-0.1$: NNS distribution $P(s)$, the cumulative spacing distribution $\int_0^s P(x)dx$, spectral rigidity $\Delta_3(L)$, and the moments of the distributions, variance $\Sigma_2(L)$, skew $\gamma_1(L)$, and excess $\gamma_2(L)$. Also shown are the results for uncorrelated random level spectra (Poisson case) and random matrix spectra (GOE). The results shown are an average over eight different spectra in various m^{π} subspaces, except for the spectral rigidity Δ_3, which has been analyzed with respect to the particular values of the z parity. Generally, a close overall agreement is observed between the present results and the predictions of random matrix theories, confirming the hypothesis of universal fluctuation patterns for classically chaotic systems. However, some deviations exist for large values of L, in particular for Δ_3 and Σ_2. These deviations are related to the breakdown of universality when L becomes larger than the internal spectral correlation length $L_{\max}$ as defined and discussed in Sec. III C [Eq. (20)].

These deviations are even more clearly shown in Fig. 3, which shows the spectral rigidity Δ_3 for a larger range of L values. Again Δ_3 is given separately for spectra belonging to positive and negative z parity. Whereas Δ_3 follows the GOE curve quite accurately up to $L=6$, the spectral rigidity soon saturates to a value which we deduce from Fig. 3 to be $\Delta_{\infty}^{+}=0.28$ and $\Delta_{\infty}^{-}=0.24$. The fact that Δ_3 converges to parity-dependent saturation values has not been observed before in any numerical exploration and is surprising at first sight. The amplitudes A_{rj} entering the semiclassical saturation formula (21) for Δ_{∞} are determined by pure classical quantities and, for unstable primitive periodic orbits r, which are traversed j times, are given here by[13,57]

$$A_{rj}^2=\frac{1/j^2}{[2\sinh(j\lambda_r/2)]^2}\ . \tag{25}$$

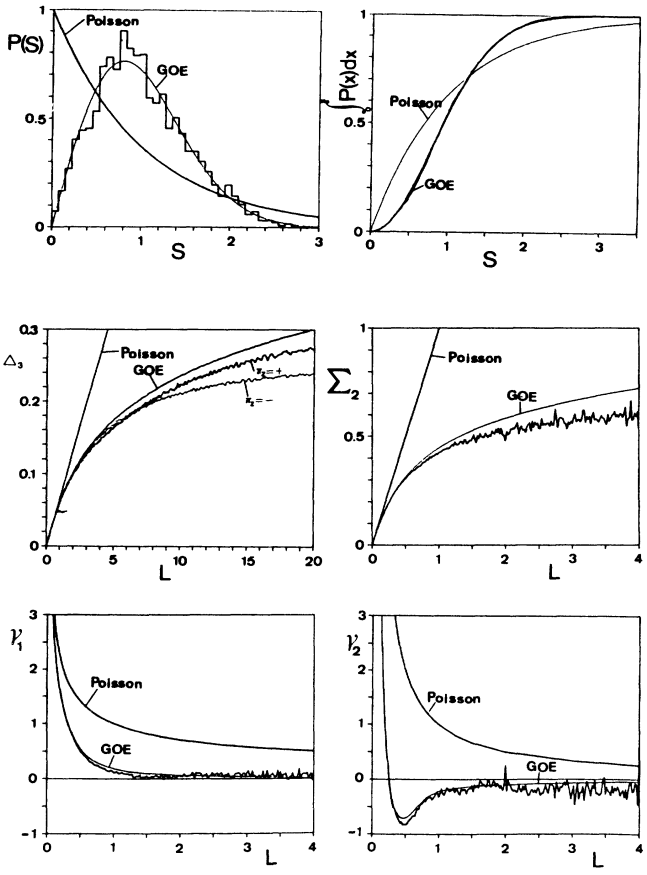

FIG. 2. Various fluctuation measures for the spectra obtained for $\varepsilon=-0.1$: nearest-neighbor spacing distribution $P(s)$, cumulative distribution $\int_0^s P(x)dx$, spectral rigidity Δ_3, number variance Σ_2, skewness γ_1, and excess γ_2. A total of 3000 calculated energy levels have entered the analysis. Also shown are the Poisson and GOE predictions.

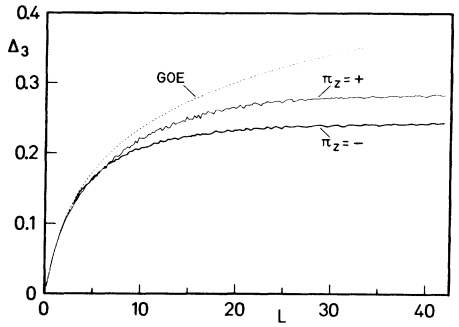

FIG. 3. Spectral rigidity Δ_3 for $\varepsilon=-0.1$ for the different z parities.

λ_r is the Liapunov exponent describing the stability of the periodic orbit t. For unstable periodic orbits which turn out to be inverse hyperbolic fixed points in the Poincaré surface of section the sinh has to be replaced by the cosh in Eq. (25).[61] (For details see, e.g., Ref. 57 and the forthcoming paper.[1]) Thus one might expect that the saturation value is independent of parity, which does not enter Eq. (25). However, in deriving Eq. (25) care has to be taken if the periodic orbit r coincides with a symmetry line of the system. This is the case for the $z\equiv 0$ periodic orbit perpendicular to the direction of the magnetic field. The sinh (or cosh) in Eq. (25) is then split in its odd and even part by expanding the sinh,

$$\frac{1}{2\sinh(x/2)}=\sum_{k=0}^{\infty} e^{-(k+1/2)x} . \tag{26}$$

$(-1)^k$ now plays the role of a local parity of the orbit. For the orbit perpendicular to the field the local orbit parity coincides with the exact z parity of the system. If we consider spectra belonging to different z parity, as is done in Fig. 3, then we have to resum Eq. (26) over odd and even k, respectively,[13,62] giving two amplitudes A_{rj}^{+} and A_{rj}^{-} differing by

$$\left[\frac{A_{rj}^{-}}{A_{rj}^{+}}\right]^2=e^{-2j\lambda_r} . \tag{27}$$

Thus the saturation value Δ_∞ becomes z-parity dependent by (and only by) the z-parity dependent contribution from the straight line periodic orbit perpendicular to the field. Putting the actual quantities into Eqs. (25) and (26) gives a parity splitting of $\Delta_\infty^{+}-\Delta_\infty^{-}=0.043$ which is close to the observed splitting of 0.040(2).

B. Level statistics in the transition regime

1. *Nearest-neighbor spacing distribution*

The nearest-neighbor spacing distribution is perhaps the most popular fluctuation measure. It is a very sensitive measure if a regular system is perturbed only slightly. In this context the behavior of the spacing distribution for small spacings is of particular interest, because it contains information of the spectrum on its finest scale (near degeneracies). In contrast to the semiclassical derivation for the spectral rigidity as described in Sec. III C, no satisfactory theory exists for the spacing distribution in the transition regime between regularity and irregularity. All that is known is that the distribution is intermediate between Poisson and Wigner, and that the distribution must vanish for spacing zero (degeneracies), reflecting the noncrossing rule of Von Neumann and Wigner.[41] Nevertheless, accidental exact degeneracies may occur,[63] but their measure is zero. Even the behavior of the distribution for small spacings is unknown and most of the proposed distributions (8)–(14) presented in Sec. III B differ in their analytic behavior at small spacings. Before we discuss the dependence of the distributions on the underlying classical dynamics, we will briefly discuss two points: first the accuracy of the multiparameter expansion (14), and second possible $\hbar$ dependencies of the spac-

ing distributions.

As an example, Fig. 4 shows the cumulative spacing distribution obtained with the spectra for $\varepsilon=-0.25$ together with the integrated fitted distribution (14) with $n_0=13$. The two curves are nearly indistinguishable not only in their overall behavior but even on a small scale. This observation also holds for n_0 equal to 12 or 14. As a further check we calculated the normalization integrals of the fitted distribution and obtained, e.g., for $n_0=13$, $\langle 1\rangle=1.0001$ and $\langle s\rangle=1.0047$. Note, that the coefficients c_n in Eq. (14) are determined by a linear fit without invoking the normalization conditions for the distribution. The fitted distribution (14) represents the smoothed "measured" spacing distribution (13) with great accuracy, so that we can get rid of the usual histogram representation. This fact will be exploited throughout this paper.

The great advantage in analyzing spectra of scale-invariant systems is that the underlying classical dynamics do not vary with energy. In all studies so far it is assumed that statistics are then stationary along the spectrum (or at least that they quickly settle down to a given distribution). Of course, proposing a distribution which should fit real spectra implicitly assumes stationarity. Although the classical dynamics of scale-invariant systems do not vary with energy, the quantum dynamics do. This can be expressed quantitatively via the commutation relations of the scaled quantum-mechanical operators associated with the scaled classical variables; for our model Hamiltonian (24) this reads, e.g.,

$$[\tilde{p}_z,\tilde{z}]=i\gamma^{1/3}\hbar\ . \tag{28}$$

At a fixed scaled energy ε determining the classical mechanics the dependence of the quantum mechanics on the magnetic field strength γ can be accounted for by an effective field strength dependent Planck's constant $\gamma^{1/3}\hbar$. Thus approaching small field strengths (or equivalently high excitation energies) leads to a small but finite effective Planck's constant. The influence of a varying effective Planck's constant on statistical measures is not known and in view of recent suggestions[48] one would also like to know whether such distributions are valid at all in the intermediate regime. Very recently a chaotic system has been analyzed in this spirit and a strong $\hbar$ dependence of statistical measures has been found.[37] $\hbar$ dependencies of spectral properties are also of interest when very weak symmetry-breaking interactions are present.[25,64]

If one assumes a statistical distribution to converge to a well-defined one, then one might expect a behavior as shown in Fig. 5(a). The figure shows the nearest neighbor spacing (NNS) distribution for four different "windows" in the $\varepsilon=-0.35$ spectra, that is each single spectrum is analyzed in four groups (windows) containing an equal amount of levels. Whereas the NNS distribution of the lowest excitation window (large effective $\hbar$) differs considerably from the other three curves, the distributions derived from higher excited windows seem to settle down quickly to a common curve (apart from some fluctuations which may be due to the finite length of the samples used). A completely different behavior is observed however, if we change the scaled energy only slightly to the value $\varepsilon=-0.30$, see Fig. 5(b). Now there is a systematic trend for avoiding small and large spacings for higher excitations and one cannot expect that the distribution containing all the four windows has settled down to the exact distribution, which we would obtain by considering *all*, in fact infinitely many, levels. As we will see later in this section, the distributions belonging to $\varepsilon=-0.3$ generally do not show the typical dependence of the distributions on the classical parameter ε. Thus Fig. 5(b) is exceptional in that it represents the most extreme $\hbar$ dependence we have observed. However, large differences between the window distributions are quite generally present when

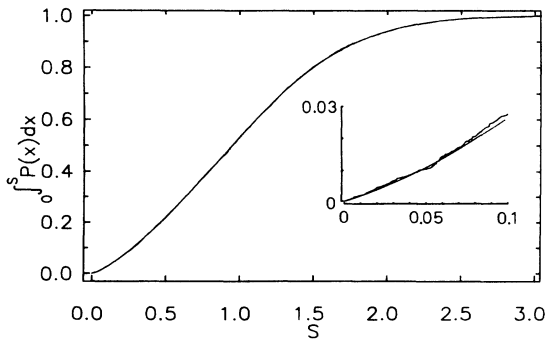

FIG. 4. Cumulative spacing distribution for $\varepsilon=-0.25$ together with the multiparameter fit (14) (smooth line), see text.

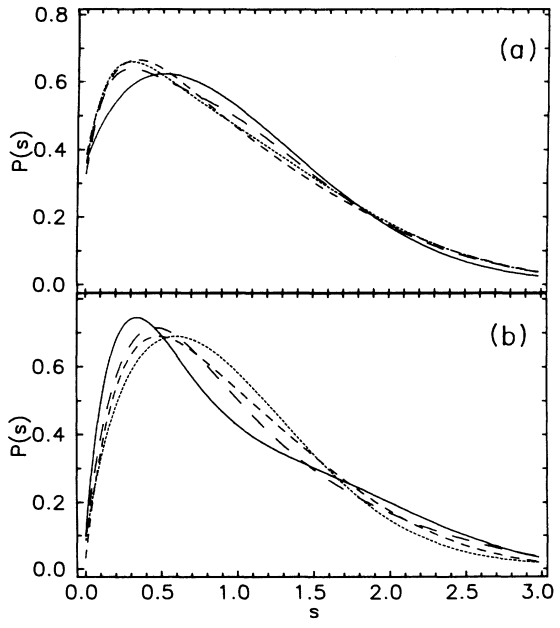

FIG. 5. Nearest-neighbor spacing distribution for (a) $\varepsilon=-0.35$ and (b) $\varepsilon=-0.30$. Each analysis is made for four different excitation windows (the shorter dashed the curves, the higher the excitations).

the classical behavior is very complex, whereas the distributions seem to approach a common curve rather quickly when the classical phase-space structure becomes simple (i.e., the system is either close to a regular *or* close to an irregular one).

We now come to the dependence of the NNS distributions on the parameter ε governing the classical dynamics. Figure 6 shows the distributions for $\varepsilon=-0.15$, -0.25, -0.35, -0.40 (solid lines), and -0.30 (dashed lines). The distribution for $\varepsilon=-0.20$ is not shown, because it is close to that of $\varepsilon=-0.25$. For the solid lines we find the expected behavior, the crossover from a Wigner-like distribution for $\varepsilon=-0.15$ to a Poisson-like distribution for $\varepsilon=-0.40$. However, as is mentioned above, the distribution for $\varepsilon=-0.3$ (dashed line) shows a different behavior than the general trend. This may be due to the fact that in this case the distribution still has not converged [see Fig. 5(b)]. In any case this behavior is surprising and its origin obscure.

A remarkable feature of the distributions is that they do not tend to zero for small spacings s. This is not an artifact related the basis set expansion (14), as we have seen in connection with Fig. 4, where the fitted curve accurately represents the real cumulative distribution even down to very small spacings. The dependence of the distributions for small spacings is shown more clearly in Fig. 7, where we plot the cumulative distributions on a double logarithmic scale. Note that the maximal spacing included is only 0.1 of the mean spacing. The slope of the curves gives information on the power-law behavior near $s=0$. Linear and quadratic dependence of the cumulative distribution corresponding to nonvanishing and vanishing spacing probability near $s=0$ are indicated on the figure. The curves obviously show quadratic dependence (linear level repulsion) for $\varepsilon=-0.10$ and $\varepsilon=-0.15$, which are both close to the Wigner distribution, but linear dependence (partly vanishing level repulsion) for the other distributions. Since we know from general grounds that $P(s)$ must be zero for $s=0$, the curves showing linear dependence must drop down somewhere, but as we can see from Fig. 7 this must appear for extremely small spacings s, which is then not noticeable on the scale of Fig. 6. Note that the curve belonging to

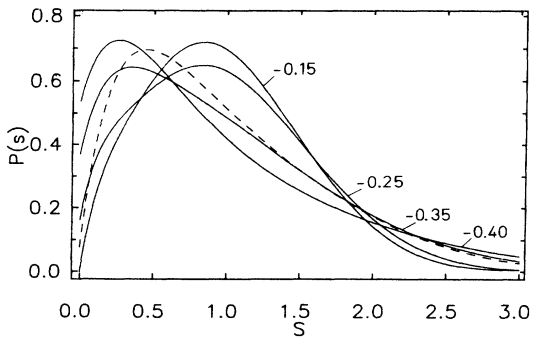

FIG. 6. Nearest-neighbor spacing distribution for different values of the scaled energy ε.

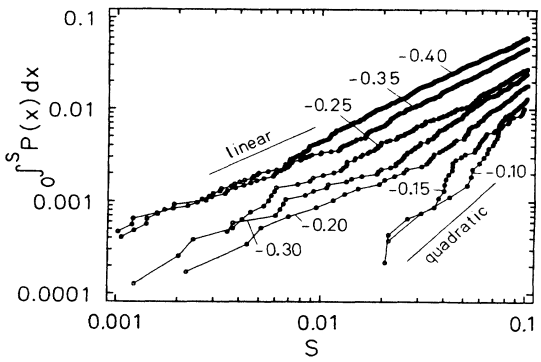

FIG. 7. Cumulative spacing distribution for small spacings for different values of the scaled energy ε. Linear and quadratic dependence on the spacing is indicated.

$\varepsilon=-0.30$ again does not conform to the general trend.

We now turn to the question of how good the spacing distributions can be imaged by one of the proposed distributions (8)–(12). As we remarked in Sec. III B 1, distribution (11) is unable to reproduce the limiting (regular) Poisson distribution and the success with distribution (12) was only limited. Although the Berry-Robnik distribution (9) is the only one having a nonvanishing probability for very small spacings, fits were generally poor. The reason for this is the pronounced minima of the observed distributions for small spacings, which cannot be reproduced with formula (9) (see also Refs. 32 and 33). Generally the best one-parameter fits were obtained with the Brody formula (8) and, unexpectedly, this formula was comparable or even better suited than the two-parameter distribution (10). This is shown in Fig. 8, where we have plotted the real distributions (solid curves) together with the best-fit Brody distributions, Eq. (8) (dotted curves), and the Hasegawa distributions, Eq. (10) (dashed curves), for three values of the scaled energy ε. The fit parameters used are tabulated in Table II. None of the distributions is able to reproduce satisfactorily the broad hump near $s=0.5$ for $\varepsilon=-0.20$ (which is also present for $\varepsilon=-0.25$, see Fig. 6), but the agreement is quite fair for $\varepsilon=-0.30$ and $\varepsilon=-0.40$. Note that the Brody distribution, although not having the correct analytic behavior near $s=0$, is particularly suited to describe the distribution for small spacings at $\varepsilon=-0.4$.

Thus from a practical point of view the Brody formula seems to be the most favorable choice for a simple parametrization of NNS data. This is in some sense unsatisfactory, first because the derivation of the formula was purely heuristic and second because the analytic behavior for very small spacings seems to be wrong (but nevertheless acceptable in practice). On the other hand the present results give some indication that the Berry-Robnik formula may become well suited in the *extreme* semiclassical limit, although it is of no great practical use for our data, even though it involves continuous sequences of the order of 10^3 levels.

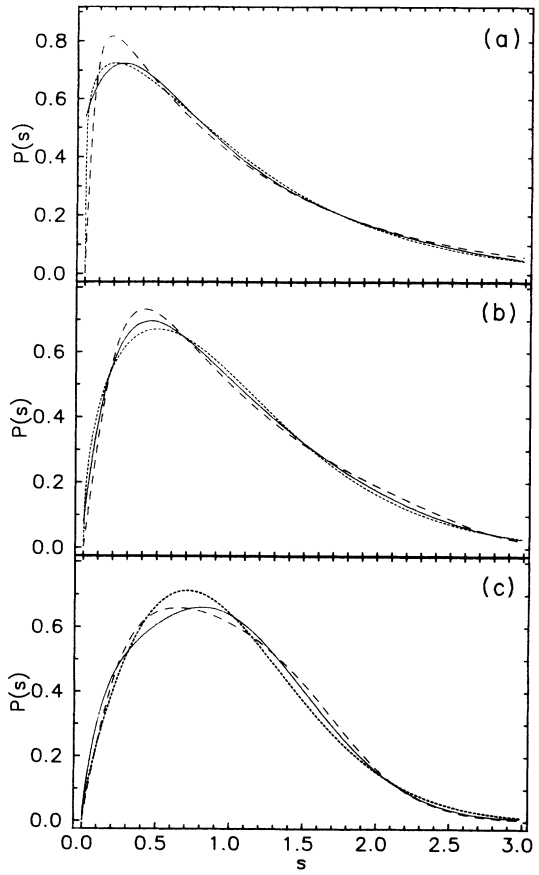

FIG. 8. Nearest-neighbor spacing distributions (solid lines) for (a) $\varepsilon=-0.4$, (b) -0.3, and (c) -0.2, together with the best fitting Brody (dotted lines) and Hasegawa distributions (dashed lines).

2. *Spectral rigidity*

Again we will discuss first the $\hbar$ dependence of the spectral rigidity described by the Δ_3 statistics. The $\hbar$ dependence is explicitly present in Eq. (21) and via the level density in the general semiclassical formula (18). For small effective $\hbar$ we have a large level density and for a large effective $\hbar$ we have a small level density. In the latter case the spectrum is more stiff as expressed by the asymptotic saturation of the spectral rigidity Δ_3, as was discussed and demonstrated in chapter V A.

Figure 9 shows the spectral rigidity Δ_3 of the $m^{\pi}=1^-$ spectrum at $\varepsilon=-0.4$ for four different windows of the spectrum. The windows are chosen such that the lowest and highest level involved are $(8n)^2$ and $[8(n+1)]^2$, $n=1,2,3,4$. With this choice the level density in the different windows is roughly proportional to n, so that the internal correlation length $L_{\max}$, defined by Eq. (20), increases linearly with n. This is represented qualitatively in Fig. 9, which shows a roughly linearly increasing saturation value of the spectral rigidity. However, the values of the internal correlation length $L_{\max}$, which are

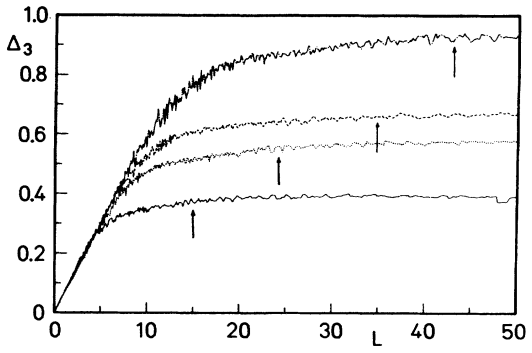

FIG. 9. Spectral rigidity Δ_3 for the $m^{\pi}=1^-$ spectrum and $\varepsilon=-0.4$. The analysis is made for four different excitation windows of the spectra (see text). The arrows indicate the L values where the semiclassical formula (20) predicts the crossover from universal to saturation behavior.

indicated by arrows in the figure, are largely overestimated by Eq. (20). The crossover from universal to saturation behavior appears for L values approximately 2–3 times smaller than $L_{\max}$. Thus, the spectrum is much more rigid than one might expect at first sight. The reason for this is that there are indeed strong correlations in the spectra on a smaller scale than $L_{\max}$ and we will see below that they are caused by the most simple stable (isolated) periodic orbits of the system.

In deriving Eq. (20) it is assumed[45] that the δ-function singularities in the density of states [discontinuities in the spectral staircase function (1)] are determined by very long orbits, whereas the short orbits give rise to the longest oscillations in the density of states [see Eq. (17)]. Then $L_{\max}$ is determined by the period of the shortest periodic orbit, which gives rise to the longest oscillation in the expansion (17) for the fluctuating part of the spectral staircase function.[45] This seems to hold (at least in most cases) for integrable systems and systems having only unstable periodic orbits, but not for generic systems. To see this we have to consider the contribution of a single stable periodic orbit to the level density. The orbit must be isolated, but this is generally fulfilled for nonintegrable systems. The orbit is then characterized by its action S, its period T, Maslov index α, and its winding number γ (or equivalently its stability angle $\nu=2\pi\gamma$)

TABLE II. Best-fit parameters q for the Brody formula (8) and best-fit parameters λ and α of the Hasegawa formula (10) obtained for the spectra of various scaled energies ε.

ε	q	λ	α
−0.15	0.95	0.17	6.0
−0.20	0.78	0.09	5.41
−0.25	0.76	0.04	8.77
−0.30	0.46	0.34	1.28
−0.35	0.36	0.11	1.66
−0.40	0.17	0.09	1.11

describing the behavior of nearby orbits. Its contribution to the level density is[13,57]

$$\frac{-iT}{\hbar}\sum_j \frac{e^{ij(S/\hbar-\alpha\pi/2)}}{2\sin(j\nu/2)} . \tag{29}$$

Evaluating the sin in Eq. (29) gives

$$\frac{-iT}{\hbar}\sum_j \sum_{k=0}^{\infty} e^{ij[S/\hbar-\alpha\pi/2-(k+1/2)\nu]} . \tag{30}$$

Equation (30) can be summed analytically to give[13,65]

$$\frac{T}{\hbar}\sum_{n,k}\delta(S/\hbar-(2\pi n+\alpha\pi/2)-(k+\tfrac{1}{2})\nu) \tag{31}$$

and a contribution to the spectral staircase function of

$$N_{\text{orbit}}(E)=\sum_{n,k}\Theta\left[\frac{S(E)}{2\pi\hbar}-\left[n+\frac{\alpha}{4}\right]-(k+\tfrac{1}{2})\gamma\right] . \tag{32}$$

The essential point now is that γ is independent of energy for scaling systems and hence Eq. (31) predicts a two-dimensional harmonic-oscillator-like level set associated with this single periodic orbit.[66] Harmonic-oscillator spectra are known to posess peculiar statistical properties, particularly being far from Poissonian. They have a regular level spacing determined by the fundamental periods of the oscillations, which modifies the assumption made in deriving $L_{\max}$, namely that the exact position of the quantum states is determined by the very long orbits. Furthermore, regular level sequences appear whose spacings are determined by the fractional part (and also by one minus the fractional part) of the winding number. Locally these sequences are indistinguishable from a level set arising from a harmonic oscillator with a frequency given by this fractional part, thus yielding a lowered internal correlation length of the spectra. By inspecting the winding numbers of the important stable orbits[66] (these are the straight line periodic orbits parallel and perpendicular to the field which we identify as the elliptic fixed points surrounded by the large elliptic islands in Fig. 1) we find that the L values for the crossover to saturation behavior should be approximately smaller by the inverse fractional part of these winding numbers, which gives roughly a factor of 2.5. These values approximately coincide with the L values where we observe saturation in Fig. 9.

Although we have seen that saturation of spectral rigidity takes place for comparatively low L values, the different window curves in Fig. 9 nearly coincide for values of L smaller than the spectral correlation length L^{cor}, which we define as the L values at the crossover from universal to saturation behavior. In this regime we expect a dependence of Δ_3 on L as described by the independent superposition of a regular and an irregular spectrum, see Eq. (15). The weights q and $1-q$ are directly related to the fraction of the regular and the irregular part of the phase space. As an example, Fig. 10 shows the best-fit curves (dotted lines) for (a) $\varepsilon=-0.25$, positive z parity, and (b) $\varepsilon=-0.40$, negative z parity. Fits were obtained by considering only the part $L\le L_0$ with $L_0=4$ ($\varepsilon=-0.25$) and $L_0=8$ ($\varepsilon=-0.4$). The agreement between the fitted and observed curves is very good up to L values 50% larger than L_0, where saturation begins to set in.

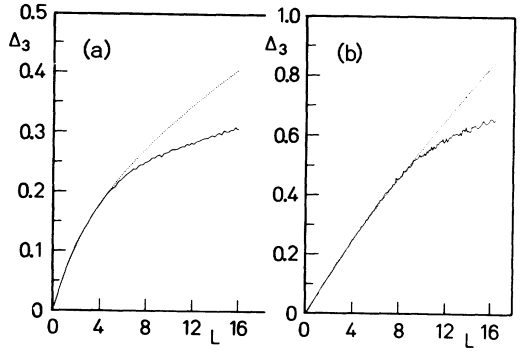

FIG. 10. Spectral rigidity Δ_3 for (a) $\varepsilon=-0.25$ and (b) $\varepsilon=-0.40$ (solid lines) and fitted curves using formula (15).

Once the fitted q values are extracted, one can compare them with the fraction q_{cl} of the regular part of the phase space. This is done in Table III. The values q_{cl} were taken from Wunner *et al.*[67] Both the classical and the fitted q values have an estimated error of ± 0.02. The close agreement between both q values is surprising when one considers that the Berry-Robnik formula (9) for the NNS distribution, whose derivation is based on the same philosophy, gives unsatisfactory results. This may be linked to the fact that Δ_3 is not so extremely sensitive to small residual interactions between regular and irregular levels as the NNS distribution.

Figure 11 now shows the spectral rigidity as calculated from the spectra for the different values of the scaled energy ε, together with the Δ_3 curves for Poisson and GOE spectra. Again we see the crossover from GOE to Poisson statistics for the nonsaturated parts of Δ_3. However, we also find here that Δ_3 for $\varepsilon=-0.30$ does not conform to the general trend: it has an extraordinary large saturation value compared to, e.g., $\varepsilon=-0.20$ and $\varepsilon=-0.35$, and a nonmonotonic behavior of its derivative. As is demonstrated in Fig. 12, this behavior arises mostly from the high-lying part of the spectrum.

TABLE III. Fractional part q_{cl} of regular classical phase space and q values obtained by fitting the spectral rigidity to Eq. (15). The estimated errors are ± 0.07 for $\varepsilon=-0.30$ and ± 0.02 otherwise.

ε	q_{cl}	q
−0.15	0.04	0.01
−0.20	0.12	0.11
−0.25	0.16	0.13
−0.30	0.24	0.17
−0.35	0.40	0.36
−0.40	0.66	0.61

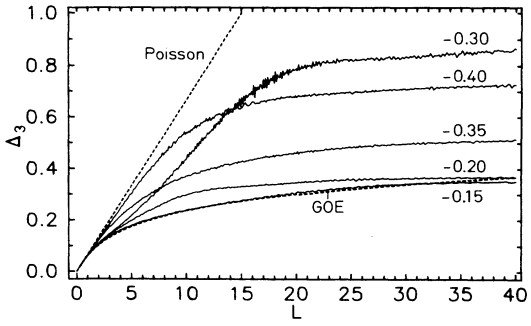

FIG. 11. Dependence of the spectral rigidity Δ_3 on the scaled energy ε.

At this stage, we will not make an attempt to explain this behavior, because it is sufficient to understand the number variance Σ_2, to which the spectral rigidity Δ_3 is related via the integral transformation (4b). This will be done in Sec. V B 3.

Finally, we discuss a point for which we have no quantitative explanation at present. The z-parity dependence of the spectral rigidity, as discussed in Sec. V A, persists even in the intermediate regime, where the symmetry orbit perpendicular to the field is stable. These splittings are tabulated in Table IV. In contrast to the case where the instability of the symmetry orbit leads to a parity-dependent magnitude of the amplitudes entering Eqs. (17) and (21), these amplitudes coincide (apart from a phase) when the orbit is stable, i.e.,

$$A_{rj}^{\pm}\frac{e^{\pm ij\nu/2}}{2j\sin(j\nu)} . \tag{33}$$

Thus the amplitudes are of same magnitude and no parity splitting should occur. We have checked the validity of Eq. (33) in different ways. First, we compared the amplitudes for $j \leq 3$ with those derived from a Fourier transform of the quantum spectra and generally found good agreement.[13] Second, the contributions to the level density including all traversals j of this orbit are a two-dimensional oscillatorlike level set, as discussed in connection with Eqs. (29)–(32). The only difference for parity then is a shift of these subspectra, which is determined solely by the stability angle ν, see Eq. (31). It is also here that we found excellent agreement with these predictions (see Ref. 1). A shift of these subspectra should have no influence on the rigidity of the complete spectra, however. A possible reason may be that the observed parity splitting is related to the termination of the sum over the transversal quantum number k in Eq. (31). The cutoff value of k is related to the size of the stable elliptic region surrounding the orbit. Thus termination of the level sets associated with the stable orbit is parity dependent.

TABLE IV. Observed parity splitting of the saturating value of the spectral rigidity Δ_3.

ε	$\Delta_\infty^+ - \Delta_\infty^-$
−0.15	0.036
−0.20	0.016
−0.25	0.008
−0.30	0.031
−0.35	−0.008
−0.40	0.008

3. *Moments of the number statistics*

In this section we will report the results obtained for the moments of the number statistics Σ_2, γ_1, and γ_2. This will be done only briefly because the results are very similar to those reported in Sec. V B 1 and V B 2. This is demonstrated, e.g., in Fig. 13, which shows the results for the number variance Σ_2. Again we observe the transition from GOE to Poissonlike statistics and the nonuniversal departures for larger L values, and again the results for $\varepsilon = -0.3$ show an extraordinary behavior. In the following we will mainly concentrate on what is different for $\varepsilon = -0.3$, which then will explain why it is extraordinary.

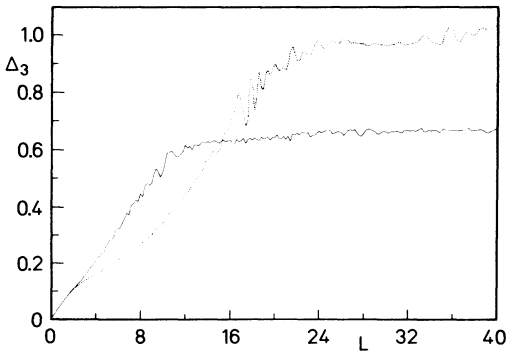

FIG. 12. Dependence of the spectral rigidity Δ_3 for $\varepsilon = -0.3$ on the excitation energy. Levels included in the analysis are 100 to 400 (solid line) and 800 to 1200 (dotted line).

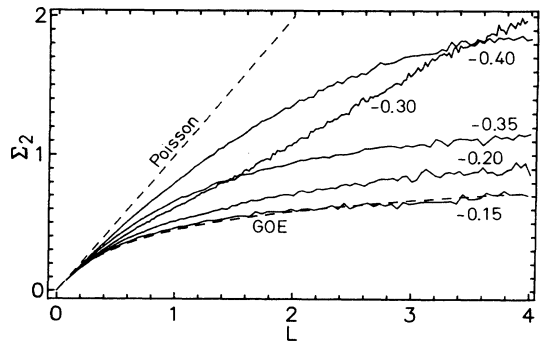

FIG. 13. Dependence of the number variance Σ_2 on the scaled energy ε.

The differences observable in Fig. 13 become more pronounced for larger L values and are shown in Fig. 14. The very fast oscillations indicate statistical errors (of course the variance itself has a variance, for example), but whereas there are only moderate modulations of the nearly constant curves for $\varepsilon=-0.25$ and $\varepsilon=-0.35$, a very pronounced sinusoidal modulation is present for $\varepsilon=-0.30$. This is even more strikingly visible in Fig. 15, showing Σ_2 for $\varepsilon=-0.3$ in the range up to $L=80$. The smooth curve in Fig. 15 is obtained by a data smoothing procedure[42] with the dotted curve for Σ_2. The wavelength of the strong modulation in Fig. 15 is determined to be $L_{\text{mod}}\approx 17.5\pm 1$.

We will show now, that the extraordinary behavior of the statistical quantities for $\varepsilon=-0.3$ is related to the level-density contribution of the symmetry orbit $z\equiv 0$ perpendicular to the magnetic field. This orbit is stable for $\varepsilon<\varepsilon_0=-0.127\,268\,612$. ε_0 defines the onset of global chaos, i.e., we have not found any stability islands in the Poincaré surfaces of section for larger values of ε,[68] see also Fig. 1. In the stable regime its stability angle ν describes the classical behavior of nearby orbits. This quantity changes its value continuously from 2π for $\varepsilon=-\infty$ down to π for $\varepsilon=\varepsilon_0$, where the elliptic fixed point associated with this orbit in the surface of section changes into an inverse hyperbolic one. In the stable regime the orbit contribution to the level density of a given m subspace is governed by Eqs. (29)–(32). When considering spectra with fixed z parity the sin in Eq. (29) has to be split in its odd and even part as discussed in connection with Eqs. (25) and (33) above. This yields the z-parity-dependent contributions

$$\frac{-iT}{\hbar}\sum_j \frac{e^{ij(S/\hbar-\alpha\pi/2\pm\nu/2)}}{2\sin(j\nu)}\ . \tag{34}$$

The essential difference between Eqs. (29) and (34) is the additional factor of 2 in the argument of the sin (the additional phase of $\nu/2$ is of minor interest in what follows). One notices that some terms in Eq. (34) become divergent when the winding number $\gamma=\nu/2\pi$ approaches a rational number. The winding numbers γ for the different values of ε are tabulated in Table V. There we find the solution for the extraordinary behavior for $\varepsilon=-0.30$, in that the winding number is very close to the low rational number $\frac{3}{4}$. Thus the amplitude (34) is extraordinary large for $j=2$ traversals of the orbit. As a consequence, the spectrum (31) consists of a two-dimensional harmonic oscillator level set with near-commensurable frequencies and hence many systematic near degeneracies. By inspecting the quantum spectra we indeed found these near-degenerate states (see Ref. 1).

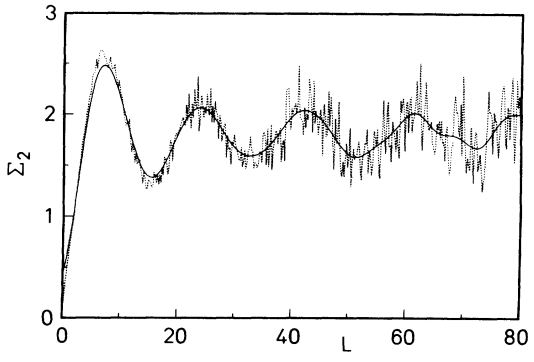

FIG. 15. Number variance Σ_2 for $\varepsilon=-0.3$ (dotted line) and its average (solid line). Levels 100 up to 1200 included.

The contributions (34) are contained, however, in the semiclassical formulas for Σ_2 and Δ_3, see Eqs. (21), (22), and (33). Now we can understand the very large saturation value of Δ_3, which essentially is the squared sum of the orbit amplitudes, divided by j times the orbit actions. In addition, the strong sinusoidal modulations of the number variance Σ_2 shown in Figs. 14 and 15 are caused by the $j=2$ term of the orbit contribution (34). This can be checked easily by inserting the actual numbers into Eq. (22). Depending on whether we choose $\bar{n}$ as the arithmetic or geometric mean of the level densities at the lower and upper bound of the spectrum involved we obtain $L_{\text{mod}}^{\text{scl}}=16.6$ and 19.8, respectively. Considering this rough estimate for the averaging of the mean level density ($\bar{n}$ varies between 17 and 60 over the whole spectrum analyzed) the agreement with the deduced value of L_{mod} is remarkably good. A further check is shown in Fig. 16, where we have plotted the smoothed variance Σ_2 ob-

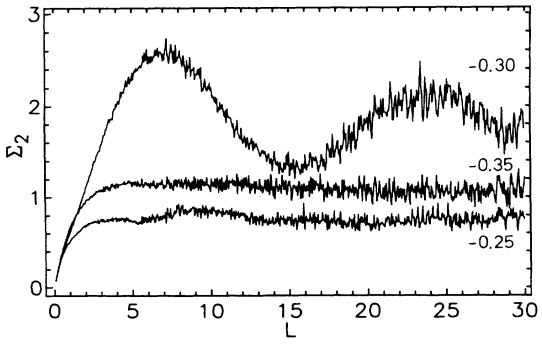

FIG. 14. Same as Fig. 13, but for larger L values.

TABLE V. Winding number γ of the periodic orbit perpendicular to the field.

ε	γ
$-\infty$	1
−0.40	0.797
−0.35	0.770
−0.30	0.740
−0.25	0.703
−0.20	0.657
−0.15	0.588
−0.127 27	0.5

tained by considering the spectra between level 600 and 1100 (solid lines). The dotted curve is the Σ_2 contribution of the periodic orbit perpendicular to the field with up to three traversals. We have taken the amplitudes from Ref. 12 and $\bar{n}$ as the level density at level 900.[69] Figure 16 shows that the strong modulations of the variance Σ_2 are indeed caused only by the periodic orbit perpendicular to the field. The agreement between the curves in Fig. 16 becomes even better when a more sophisticated average of the mean level density $\bar{n}$ is chosen.[70] Thus all the observed extraordinary features in the spectral statistics for $\varepsilon=-0.30$ are linked to the accidentally low resonant value of the winding number γ for the stable periodic orbit perpendicular to the field.

In the light of these results one is not surprised to find similar effects for the higher moments of the distributions, and for completeness we show results in Fig. 17 for γ_1 and in Fig. 18 for γ_2. What is noteworthy is that the transition to Poisson statistics is much slower than for the other statistical measures analyzed so far, particularly for L values larger than 2.5. Furthermore, for $L>2$ all curves for γ_2 are below the GOE prediction and thus *not* intermediate between GOE and Poisson. Again the behavior for $\varepsilon=-0.3$ is abnormal and pronounced modulations with the same wavelength as for Σ_2 are again present as predicted by semiclassical formulas[43] (see Fig. 19 for γ_1).

VI. SUMMARY AND CONCLUSIONS

To summarize we have studied the fluctuation properties of large scale quantum spectra derived from the classically scale-invariant Hamiltonian describing the hydrogen atom in a uniform magnetic field. The data presented are of a statistical significance hitherto not achieved by any other study of these topics. We particularly focussed on the dependence of the fluctuation properties on the parameter ε governing the transition from regularity to irregularity in the classical system.

The most important conclusion that can be drawn from the present analysis is a definite statement concerning the question: Suppose we know the global structure of the classical phase space. Does this knowledge allow us to make any quantitative prediction concerning the associated quantum spectra?[71] As we have seen in Sec. V this is generally *not* the case, but a more *detailed* knowledge of the classical dynamics is necessary. Only for systems whose classical motion is dominated by global chaos or by complete regularity (integrability) such predictions seem to be possible (universal fluctuation properties).

As was demonstrated in Sec. V all the statistical measures are strongly influenced by the presence of stable periodic orbits surrounded by large elliptic islands in phase space. This includes (i) a significantly lowered value of where spectral rigidity saturation sets in and (ii) extraordinary behavior of all statistical measures when the winding numbers of certain periodic orbits are close to low rationals.

Although we cannot prove (ii) for the NNS it seems reasonable that the observed deviations are also linked to the presence of harmonic-oscillator-like level sets in the spectra. Considering that no spacing distribution exists for harmonic oscillators,[72] we conclude that there is *no universal* family of NNS distributions for the transition

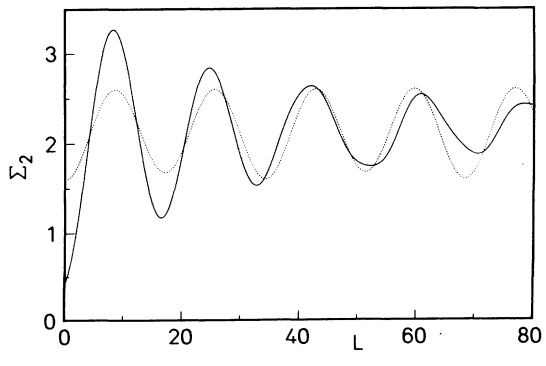

FIG. 16. Smoothed number variance Σ_2 for $\varepsilon=-0.3$ (solid line, levels 600 up to 1100 included), and the semiclassical contribution of the periodic orbit perpendicular to the field to Σ_2, see text.

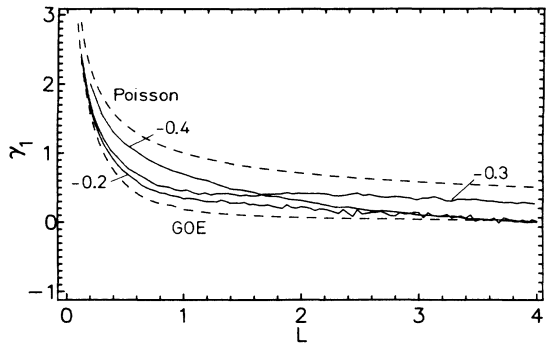

FIG. 17. Dependence of the skewness γ_1 on the scaled energy ε.

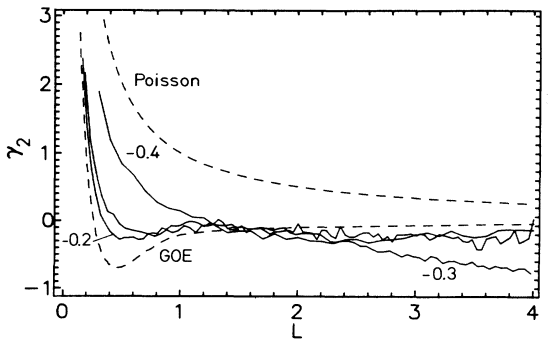

FIG. 18. Dependence of the excess γ_2 on the scaled energy ε.

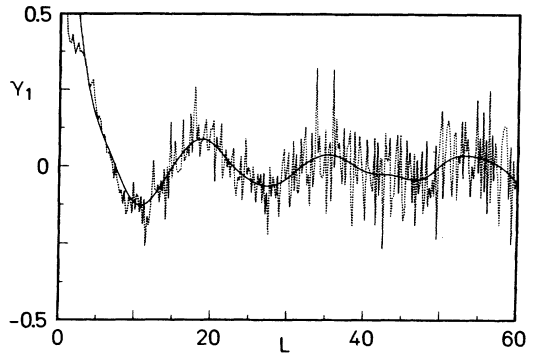

FIG. 19. Skewness γ_1 for $\varepsilon = -0.3$ (dotted line) and its average (solid line).

regime between regularity and irregularity. We can expect at best that NNS distributions are close to a family of common distributions interpolating between Poisson and Wigner, but the deviations from such common curves can be large. This may also explain why the Berry-Robnik formula (9) fails to parametrize the spacing distributions: the regular part of the spectra can be far from Poissonian.

Finally, we remark on the generality of the present results. As was shown, the presence of stable periodic orbits surrounded by large elliptic islands gives rise to a d-dimensional harmonic-oscillator-like level set ($d=2$ in our case) embedded in the complete spectrum. This is a generic property of *all scale-invariant* Hamiltonian systems. The observed extraordinary behavior is related to the nongeneric statistical behavior of harmonic oscillators and *not* to the fact that levels exist which are associated with the regular part of the phase space. For nonscaling systems the winding numbers become explicitly energy dependent. As a consequence the regular part of the spectrum will deviate strongly from a harmonic-oscillator-like pattern. Scaling systems are nongeneric with respect to this and for nonscaling systems we expect absence of extreme extraordinary behavior. Unfortunately this can hardly be proved because the phase-space structure is varying in any case for nonscaling systems and this effect must be controlled separately. The best way to test this hypothesis would be to consider a system with one dominantly contributing stable periodic orbit, for which the winding number of the nearby orbits varies strongly. This also leads to strong deviations from a harmonic-oscillator-like level set associated with the periodic orbit.

ACKNOWLEDGMENTS

This work was supported in part by the Deutsche Forschungsgemeinschaft. We gratefully acknowledge fruitful discussions with J. S. Briggs, O. Bohigas, and J. J. M. Verbaarschot.

[1]A. Honig and D. Wintgen (unpublished).
[2]*Atomic Spectra and Collisions in External Fields 2,* edited by K. T. Taylor *et al.* (Plenum, New York, 1988).
[3]H. Friedrich and D. Wintgen, Phys. Rep. (to be published).
[4]A. Holle, G. Wiebusch, J. Main, B. Hager, H. Rottke, and K. H. Welge, Phys. Rev. Lett. **56**, 2594 (1986).
[5]J. Main, G. Wiebusch, A. Holle, and K. H. Welge, Phys. Rev. Lett. **57**, 2789 (1986).
[6]A. Holle, J. Main, G. Wiebusch, H. Rottke, and K. H. Welge, Phys. Rev. Lett. **61**, 161 (1988).
[7]D. Wintgen and H. Friedrich, Phys. Rev. Lett. **57**, 571 (1986).
[8]D. Delande and J. C. Gay, Phys. Rev. Lett. **57**, 2006 (1986).
[9]G. Wunner, U. Woelk, I. Zech, G. Zeller, T. Ertl, F. Geyer, W. Schweitzer, and H. Ruder, Phys. Rev. Lett. **57**, 3261 (1986).
[10]D. Wintgen, Phys. Rev. Lett. **58**, 1589 (1987).
[11]M. L. Du and J. B. Delos, Phys. Rev. Lett. **58**, 1731 (1987); Phys. Rev. A **38**, 1896 (1988); **38**, 1913 (1988).
[12]D. Delande and J. C. Gay, Phys. Rev. Lett. **59**, 1809 (1987).
[13]D. Wintgen, Phys. Rev. Lett. **61**, 1803 (1988).
[14]D. Wintgen, A. Holle, G. Wiebusch, J. Main, H. Friedrich, and K. H. Welge, J. Phys. B **19**, L557 (1986).
[15]A. Holle, G. Wiebusch, J. Main, K. H. Welge, G. Zeller, G. Wunner, T. Ertl, and H. Ruder, Z. Phys. D **5**, 279 (1987).
[16]P. Cacciani, E. Luc-Koenig, J. Pinard, C. Thomas, and S. Liberman, J. Phys. B **19**, L519 (1986).
[17]J. Neukammer, H. Rinneberg, K. Vietzke, A. König, H. Hieronymus, M. Kohl, H.-J. Grabka, and G. Wunner, Phys. Rev. Lett. **59**, 2947 (1987).
[18]P. F. O'Mahony and K. T. Taylor, Phys. Rev. Lett. **57**, 2931 (1986).
[19]O. Bohigas, M. Giannoni, and C. Schmit, Phys. Rev. Lett. **52**, 1 (1984).
[20]N. Rosenzweig and C. E. Porter, Phys. Rev. **120**, 1698 (1966).
[21]R. U. Haq, A. Pandey, and O. Bohigas, Phys. Rev. Lett. **48**, 1086 (1982).
[22]H. S. Camarada and P. D. Georgopulos, Phys. Rev. Lett. **50**, 492 (1983).
[23]O. Bohigas, R. U. Haq, and A. Pandey, Phys. Rev. Lett. **54**, 1645 (1985).
[24]Th. Zimmermann, H. Köppel, L. S. Cederbaum, G. Persch, and W. Demtröder, Phys. Rev. Lett. **61**, 3 (1988).
[25]G. E. Mitchell, E. G. Bilpuch, P. M. Endt, and J. F. Shriner, Phys. Rev. Lett. **61**, 1473 (1988).
[26]G. R. Welch, M. M. Kash, C. Ju, L. Hsu, and D. Kleppner, Phys. Rev. Lett. **62**, 893 (1989).
[27]There are now so many theoretical studies that we can only refer to review articles; see e.g., O. Bohigas, M.-J. Giannoni, and C. Schmit, Lect. Notes Phys. **263**, 18 (1986); B. Eckhardt, Phys. Rep. **163**, 205 (1988).
[28]E. Haller, H. Köppel, and L. S. Cederbaum, Phys. Rev. Lett. **52**, 1665 (1984); H. D. Meyer, E. Haller, H. Köppel, and L. S. Cederbaum, J. Phys. A **17**, L813 (1984); T. Zimmermann, H.-D. Meyer, H. Köppel, and L. S. Cederbaum, Phys. Rev. A **33**, 4334 (1986).
[29]T. H. Seligman, J. J. M. Verbaarschot, and M. R. Zirnbauer, Phys. Rev. Lett. **53**, 215 (1984); T. H. Seligman and J. J. M. Verbaarschot, J. Phys. A **18**, 2227 (1985).
[30]E. Caurier and B. Grammaticos, Europhys. Lett. **2**, 417 (1986).

[31]H. Frahm and H. J. Mikeska, Z. Phys. B **65**, 249 (1986); F. M. Izrailev, Novosibirsk Report No. 88-45, 1988 (unpublished).
[32]D. Wintgen and H. Friedrich, Phys. Rev. A **35**, 1464 (1987).
[33]J. Reichl and H. Büttner, J. Phys. A **20**, 6321 (1987).
[34]A. J. Lichtenberg and M. A. Lieberman, *Regular and Stochastic Motion* (Springer, New York, 1983).
[35]D. A. Harmin, Phys. Rev. A **26**, 2656 (1982).
[36]M. C. Gutzwiller, J. Math. Phys. **18**, 806 (1977).
[37]D. Wintgen and H. Marxer, Phys. Rev. Lett. **60**, 971 (1988).
[38]O. Bohigas and M.-J. Giannoni, in *Mathematical and Computational Methods in Nuclear Physics,* Vol. 209 of *Lecture Notes in Physics,* edited by J. S. Dehesa, J. M. G. Gomez, and A. Polls (Springer, Berlin, 1984), p. 1.
[39]O. Bohigas and H. A. Weidenmüller, Ann. Nucl. Phys. (to be published).
[40]*Quantum Chaos and Nuclear Statistical Physics,* Vol. 263 of *Lecture Notes in Physics,* edited by T. H. Seligman and H. Nishioka (Springer, Berlin, 1986).
[41]M. V. Berry, in *Chaotic Behavior of Deterministic Systems, Proceedings of the Les Houches Summer School, Session XXXVI,* edited by G. Iooss, R. H. G. Helleman, and R. Stora (North-Holland, Amsterdam, 1983), p. 171.
[42]*Numerical Recipes,* edited by W. H. Press, B. P. Flannery, S. A. Teukolsky, and W. T. Vetterling (Cambridge University Press, Cambridge, 1986).
[43]J. J. M. Verbaarschot, J. Phys. A **20**, 5589 (1987).
[44]T. A. Brody, J. Flores, J. B. French, P. A. Mello, A. Pandy, and S. S. M. Wong, Rev. Mod. Phys. **53**, 385 (1981).
[45]M. V. Berry, Proc. R. Soc. London, Ser. A **400**, 229 (1985).
[46]M. V. Berry and M. Robnik, J. Phys. A **19**, 649 (1986); **19**, 669 (1986).
[47]M. Henon, Ref. 41, p. 53.
[48]M. Robnik, J. Phys. A **20**, L495 (1987).
[49]T. A. Brody, Lett. Nuovo Cimento **7**, 482 (1973).
[50]M. V. Berry and M. Robnik, J. Phys. A **17**, 2413 (1984).
[51]H. Hasegawa, H. J. Mikeska, and H. Frahm, Phys. Rev. A **38**, 395 (1988); H. Hasegawa, in Ref. 1.
[52]P. Pechukas, Phys. Rev. Lett. **51**, 943 (1983).
[53]T. Yukawa, Phys. Rev. Lett. **54**, 1883 (1985).
[54]*Handbook of Mathematical Functions,* edited by M. Abramowitz and I. A. Stegun (Dover, New York, 1965).
[55]J. J. M. Verbaarschot (private communication); T. Guhr (private communication).
[56]M. V. Berry, Nonlinearity **1**, 399 (1988).
[57]M. C. Gutzwiller, J. Math. Phys. **12**, 343 (1971); Phys. Rev. Lett. **45**, 150 (1980); Physica (Amsterdam) **5D**, 183 (1982).
[58]J. H. Hannay and A. M. Ozorio de Almeida, J. Phys. A **17**, 3429 (1984).
[59]D. Wintgen and H. Friedrich, Phys. Rev. A **36**, 131 (1987).
[60]G. Wunner *et al.* (private communication).
[61]M. Tabor, Physica (Amsterdam) **6D**, 195 (1983).
[62]D. Wintgen, J. Phys. B **22**, L5 (1989).
[63]H. Friedrich and D. Wintgen, Phys. Rev. A **31**, 3964 (1985).
[64]D. Boose, H. L. Harney, and H. A. Weidenmüller, Phys. Rev. Lett. **56**, 2012 (1986); J. B. French, V. K. B. Kota, A. Pandey, and S. Tomsovic, Phys. Rev. Lett. **58**, 2400 (1987).
[65]W. H. Miller, J. Chem. Phys. **63**, 996 (1975).
[66]The validity range of Eq. (31), in particular restrictions on the range of k, depends strongly on the size of the elliptic island surrounding the stable fixed point, but this does not alter the argumentation below.
[67]G. Wunner, G. Zeller, U. Woelk, W. Schweizer, R. Niemeier, F. Geyer, H. Friedrich, and H. Ruder, in Ref. 1.
[68]Stable orbits exist, however, even for $\varepsilon_0 < \varepsilon < 0$, but the size of the elliptic islands surrounding these orbits are negligibly small; see D. Wintgen, J. Phys. B **20**, L511 (1987), and Ref. 2.
[69]A constant has been added to shift the semiclassical curves for Σ_2. Note that in this case the action S_r repalces the role of the time T_r in Eq. (22).
[70]A. Hönig, Diploma thesis, Universität Freiburg, 1989.
[71]This is of course the extended version of the conjecture mentioned in Sec. III A.
[72]A. Pandey, O. Bohigas, and M. J. Giannoni (unpublished).

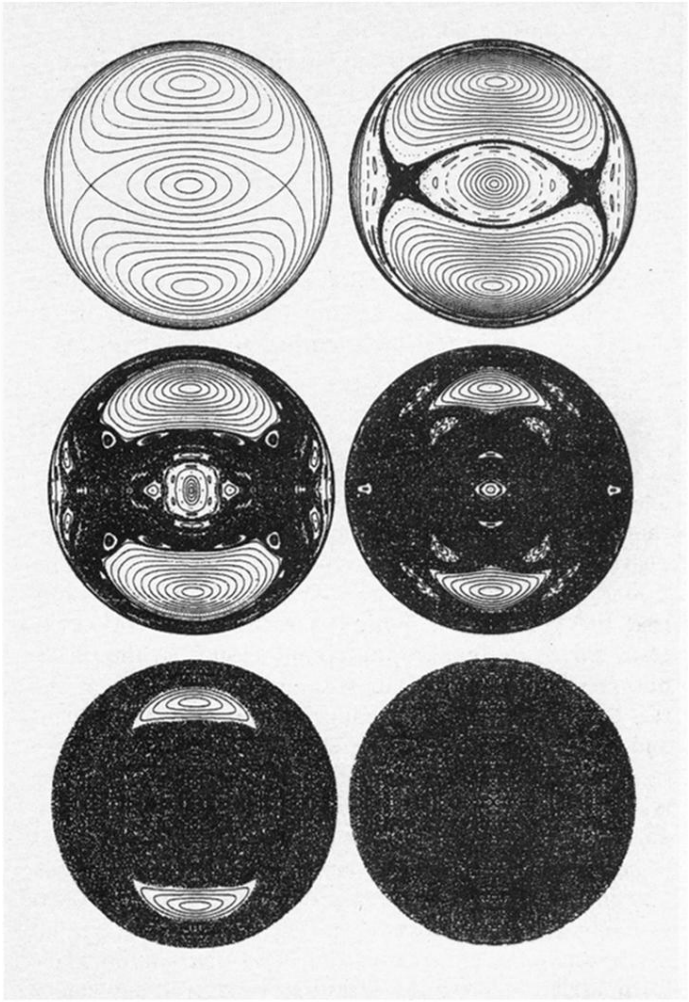

FIG. 1. Poincaré surfaces of section for the hydrogen atom in a uniform magnetic field for different values of the scaled energy ε: -0.8, -0.5, -0.4, -0.3, -0.2, and -0.1 (from left to right and top to bottom).